Materials Science and Engineering C 50 (2015) 37–44

Contents lists available at ScienceDirect

Materials Science and Engineering C

journal homepage: www.elsevier.com/locate/msec

# Surface modification of Ni–Ti alloys for stent application after magnetoelectropolishing

Puneet Gill [a,*], Vishal Musaramthota [a], Norman Munroe [a], Amit Datye [b], Rupak Dua [d], Waseem Haider [c], Anthony McGoron [d], Ryszard Rokicki [e]

[a] Department of Mechanical and Materials Engineering, Florida International University, Miami, FL 33174, USA
[b] Department of Materials Science and Engineering, The University of Tennessee, Knoxville, TN 37916, USA
[c] Mechanical Engineering, University of Texas-Pan American, TX, USA
[d] Department of Biomedical Engineering, Florida International University, Miami, FL 33174, USA
[e] Electrobright, Macungie, PA 18062, USA

ARTICLE INFO

*Article history:*
Received 9 May 2014
Received in revised form 2 November 2014
Accepted 4 January 2015
Available online 7 January 2015

*Keywords:*
Nitinol
Magnetoelectropolishing
SEM/EDS
XPS
Nanoindentation
Endothelial cells

ABSTRACT

The constant demand for new implant materials and the multidisciplinary design approaches for stent applications have expanded vastly over the past decade. The biocompatibility of these implant materials is a function of their surface characteristics such as morphology, surface chemistry, roughness, surface charge and wettability. These surface characteristics can directly influence the material's corrosion resistance and biological processes such as endothelialization. Surface morphology affects the thermodynamic stability of passivating oxides, which renders corrosion resistance to passivating alloys. Magnetoelectropolishing (MEP) is known to alter the morphology and composition of surface films, which assist in improving corrosion resistance of Nitinol alloys. This work aims at analyzing the surface characteristics of MEP Nitinol alloys by scanning electron microscopy (SEM) and X-ray photoelectron spectroscopy (XPS). The wettability of the alloys was determined by contact angle measurements and the mechanical properties were assessed by Nanoindentation. Improved mechanical properties were observed with the addition of alloying elements. Cyclic potentiodynamic polarization tests were performed to determine the corrosion susceptibility. Further, the alloys were tested for their cytotoxicity and cellular growth with endothelial cells. Improved corrosion resistance and cellular viability were observed with MEP surface treated alloys.



## 1. Introduction

It is projected that by 2015, there will be 133 million Americans over the age of 45, at which the incidence of heart diseases increases [1]. Many of such patients will receive non-surgical treatment requiring the installation of stents to open blocked heart arteries via angioplasty [2]. Stents are tiny expandable mesh tubes that may be bare metal or polymer coated for drug delivery and serve as permanent scaffolds for the newly opened arteries. However, bare metal stents have been fraught with the occurrence of restenosis (re-blockage of arteries) after angioplasty [3]. *In-stent* restenosis, which results in the growth of scar tissue in the areas of contact between the material and the surface of the blood vessel that eventually leads to its blockage, occurs usually 3 to 6 months after implantation [4]. Drug eluting stents (DES) are coated with medication that is slowly released (eluted) to help prevent the growth of scar tissue in the artery lining. However, DES require longer treatment with blood thinners to prevent closure from clotting (thrombosis). In this multi-billion dollar industry, with over 3 million patients worldwide, stainless steel (SS316) and cobalt chromium (CoCr) alloys have been extensively used for the manufacture of stents and it is estimated that 15% of all stents are manufactured from Nitinol (NiTi) and CoCr alloys [5]. Recently, there has been a decline in revenues generated as a result of complications from thrombosis and restenosis [6,7]. Thrombosis sometimes results in death or large non-fatal myocardial infarction (MI) with an estimate of less than 10% diagnosed for cardiac deaths [8–10]. Thus, the Food and Drug Administration, the American Heart Association and others call for a new generation of stents that are more flexible and adaptable to arteries. The future of biomaterials, therefore, depends on a better understanding of mechanisms by which they can be rendered stable and inert but yet retain flexibility, machinability and good biocompatibility.

The performance of an implant is mainly determined by its physiochemical properties. The major concern with metallic implant materials is their corrosion behavior which is influenced by many factors including their chemical composition, surface conditions, microstructure and oxygen content, pH and temperature of the surrounding environment [11]. Recently, a significant amount of attention has been focused on the surface modification of Nitinol alloys in an effort to enhance their corrosion resistance and biocompatibility. Various surface treatments

* Corresponding author.

http://dx.doi.org/10.1016/j.msec.2015.01.009
0928-4931/

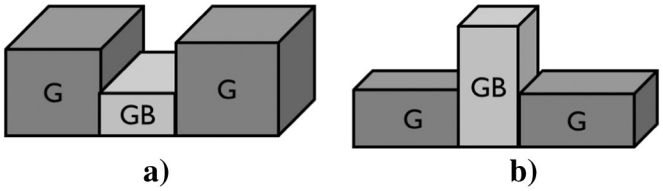


**Fig. 1.** G represents Grain and GB represents Grain Boundary (a) depressed grain boundaries and elevated grains in Ni–Ti–Cr and b) depressed grains and elevated grain boundaries in Ni–Ti–Ta.

have been adopted, including mechanical and electrochemical treatments [12], chemical etching, heat treatments, conventional and plasma ion immersion implantation [13], laser and electron-beam irradiation and application of bioactive surfaces [14]. Kun Zhang et al. provided an in-depth review of various vascular stent surface modifications and their role on enhancing biological properties by primarily focusing on endothelialization on stent materials [15].

The main intent of vascular stent surface modification techniques is to produce a uniform, stable and highly adherent $TiO_2$ rich layer. Chu et al. reported a new surface modification technique, which encompassed the electropolishing (EP) pretreatment and photoelectrocatalytic oxidation (PEO) of Nitinol [16] after which a nickel free $TiO_2$ layer was observed with a graded interfacial layer between the surface and Nitinol substrate. This surface modification proved to be very effective in suppressing nickel leaching during a 10 week immersion test [16]. Zhang et al. reported that coating Nitinol with Titanium Nitride (TiN) reduced its corrosion rate by 50% and nickel leaching by 35% in simulated blood plasma [18]. However, the coating cracked when deformation was greater than 4% [17,18]. Additionally, Shabalovskaya et al. compared corrosion resistance of sandblasted and fine-drawn Nitinol wires, and also observed the effect of electropolishing, on corrosion behavior of these wires. A low corrosion resistance was observed for both sandblasted and fine-drawn Nitinol wires, which was attributed to inclusions within the surface, which were present in the bulk [19]. Henceforth, a homogenous superior surface is always interdependent on its subsurface.

**Table 1**
Nominal and analyzed compositions of the alloys used in this study (in atomic percent).

| Alloys | Nominal | | | | | EDS compositions | | | | |
|---|---|---|---|---|---|---|---|---|---|---|
| | Ni | Ti | Ta | Cr | O | Ni | Ti | Ta | Cr | O |
| *NiTi* | Balance | 49 | NA | NA | NA | Balance | 47 | NA | NA | 7 |
| *NiTi10Ta* | Balance | 44 | 10 | NA | NA | Balance | 45 | 7 | NA | 6 |
| *NiTi10Cr* | Balance | 44 | NA | 10 | NA | Balance | 42 | NA | 8 | 10 |

Alloying and surface treatments change the aforementioned surface characteristics, which in turn affect the biocompatibility of implant materials [15]. Dharam et al. reported that alloyed Nitinol subjected to electropolishing (EP) and magnetoelectropolishing (MEP) could result in improved cellular adhesion and enhance endothelialization [20]. Haider et al. reported that MEP treated alloyed Nitinol was highly corrosion resistant to pitting and crevice corrosion [21].

In this current research, the effect of alloying with Ta and Cr and MEP treatment of Nitinol were investigated. Ta, a heavy element, improves the radiopacity of Nitinol whereas Cr has been found to not only improve the corrosion resistance of Nitinol but also to enhance endothelial cell growth [22]. The principle behind MEP is dependent on a very strong interaction between an externally applied magnetic field and ferromagnetic elements such as Fe, Ni, and Co during the electrolytic process. In the MEP of Nitinol, ferromagnetic nickel corrodes disproportionately faster than paramagnetic titanium as a result of the applied magnetic field so that a nickel free oxide layer is formed [23]. In order

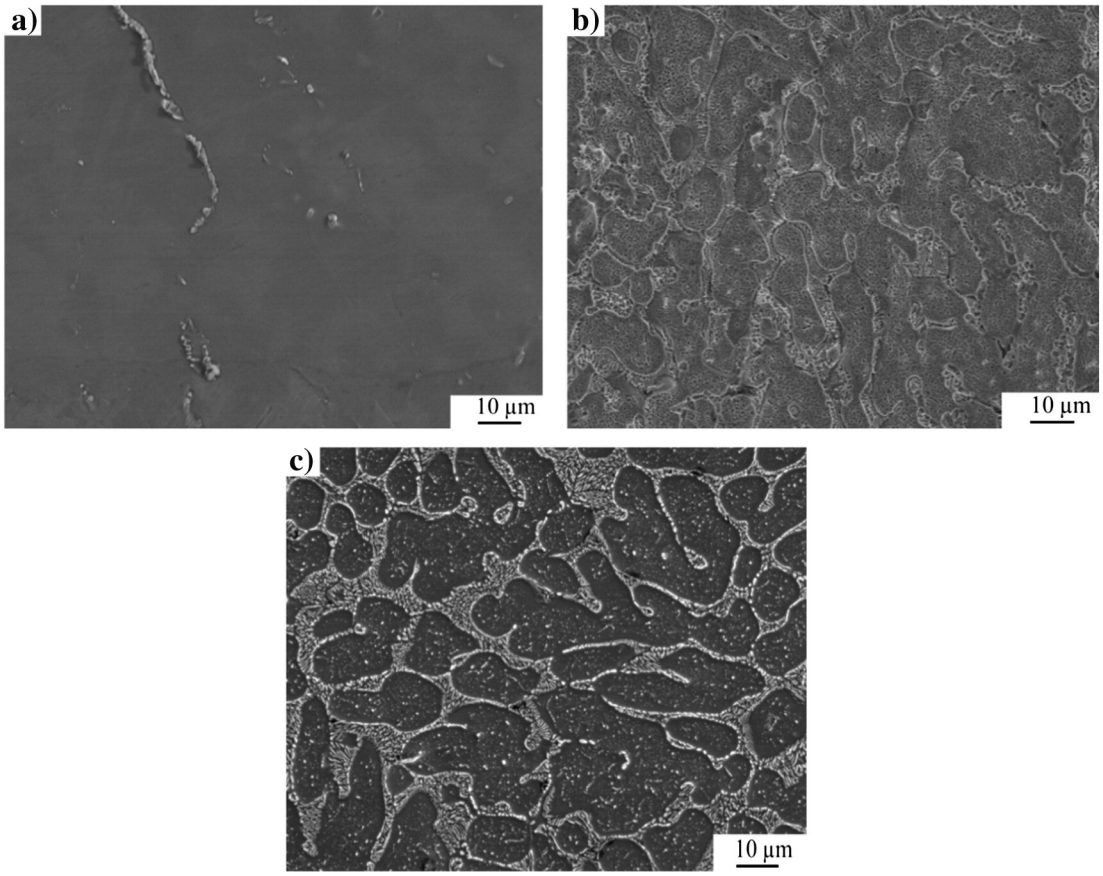


**Fig. 2.** SEM photomicrographs of MEP alloys: (a) NiTi, (b) Ni–Ti–Ta and (c) Ni–Ti–Cr [22].

**Table 2**
Surface oxide concentration (at.%) and thickness (nm) of MEP Nitinol alloys detected using XPS (ND = not detected and NA = not applicable).

| Alloys | $TiO_2$ | $Ni_2O_3$ | $Cr_2O_3$ | $Ta_2O_5$ | Ti/Ni | Oxide thickness (nm) |
|---|---|---|---|---|---|---|
| NiTi | 6.5 | 1.1 | NA | NA | 2.2 | 18.2 |
| NiTi10Ta | 11.7 | ND | NA | 2.4 | 8.5 | 10.4 |
| NiTi10Cr | 6.0 | 1.7 | 2.0 | NA | 3.3 | 11.0 |

**Table 4**
Kitazaki-Hata surface free energy components ($mJ/m^2$).

| Alloy | Dispersion (d) | Polar (p) | Hydrogen component (h) | Fractional polarity (FP) | Surface free energy ($mJ/m^2$) |
|---|---|---|---|---|---|
| NiTi | 27.4 | 8.8 | 1.8 | 0.2 | 38.0 |
| NiTi10Ta | 20.5 | 3.5 | 0.7 | 0.2 | 24.7 |
| NiTi10Cr | 22.4 | 1.4 | 0.0 | 0.1 | 23.8 |

to further assess the effect of alloying on the corrosion behavior of Nitinol, cyclic potentiodynamic polarization studies were performed in phosphate buffer saline solution (PBS) [24]. Conjointly, the cytotoxicity of the ions released during the corrosion studies on endothelial cells was evaluated by Sulforhodamine-B (SRB) assay, which is based on a calorimetric measurement of cellular protein content. Additionally, cell growth on the surface of the alloys was visualized using a mitochondrial and nuclear labeling kit. The Mitotracker Red dye provided highly selective mitochondrial staining whereas the blue hoechst dye provided staining for the nuclei. Scanning electron microscopy (SEM) and X-ray photoelectron spectroscopy (XPS) were utilized to characterize the effect of alloying and MEP on surface morphology and surface chemistry.

## 2. Materials and methods

### 2.1. Sample preparation

Binary and ternary Nitinol alloys were prepared by arc melting at the National Institute of Standards and Technology (NIST). Ingots were cut into cylindrical discs of dimension 1 cm × 1 cm area and 2 mm thick using a linear precision high speed saw (ISOMET 4000). Samples were mechanically polished using silicon carbide abrasive grit papers 240, 320, 400 and 600 sequentially followed by 1 μm, 0.5 μm and 0.05 μm alumina polishing media.

The polished samples were then subjected to MEP (Electrobright®, Macungie, PA, USA). MEP utilizes identical conditions of the conventional EP process, except for the imposition of an externally applied magnetic field created using four ring magnets stacked around the electrochemical cell. The magnetic field of about 100 mT was directed parallel to the work-piece surface (sample). The effect of the Lorenz force was visually observed by circular movement of the electrolyte around the sample during the MEP process.

### 2.2. X-ray photoelectron spectroscopy

XPS provided both qualitative and quantitative data on the surface composition of all materials. A PHI Quantera scanning XPS microprobe employing a monochromatic Al $K_\alpha$ X-ray radiation was utilized. Wide energy survey spectra were collected in a large area analysis mode to determine which elements were present at the surface. The large area analysis mode probed an area 100 × 1500 μm with a 100 W monochromatic Al Ka X-ray beam. Sputter depth profiles were obtained using the large area analysis mode and 2 kV argon ions rastered over a 3 × 3 mm area. A sputter etch rate of 6.5 nm/min was determined using a $SiO_2$ film of known thickness. Zalar rotation was used to minimize sputter induced artifacts that might broaden detected interfaces. The composition stabilized at a depth of 100 to 300 nm below the surface.

**Table 3**
Average values from the acid–base theory of contact angle, interfacial free energy and work of adhesion.

| Alloy | Contact angle (degree) | Interfacial free energy ($mJ/m^2$) | Work of adhesion ($mJ/m^2$) |
|---|---|---|---|
| NiTi | 83.8 | 26.0 | 80.7 |
| NiTi10Ta | 94.7 | 33.5 | 64.0 |
| NiTi10Cr | 105.9 | 42.8 | 53.8 |

### 2.3. Scanning electron microscopy/energy dispersive spectroscopy

SEM was employed to determine the surface morphology of the specimen. A JOEL JSM 5900 LV equipment containing a $LaB_6$ filament at an excitation voltage of 20 kV in secondary electron mode was utilized. EDS measurements were conducted to assess the elemental composition and homogeneity. In this regard, various locations on the samples were examined under different magnifications.

### 2.4. Wettability

Contact angles were measured under ambient conditions using a Kyowa contact angle meter, model DM-CE1 by adopting the sessile drop method. Three different solvents (water, ethylene-glycol and diiodomethane) of various surface tensions were utilized. Ten tests were performed with each solvent on each specimen at locations separated by sufficient spacing (~0.5 mm) to prevent any interference from the previous tests. A FAMAS analysis software was employed to evaluate the surface free energy (SFE) in terms of the contact angle θ, the surface tension of the liquid σl and the interfacial tension γsl between liquid and solid according to the Young's Equation ($\sigma_s = \gamma_{sl} + \sigma_s \cdot \cos$ ) as well as the work of adhesion ($W_a = \sigma_s + \sigma_l - \sigma_{sl}$), where $\sigma_s$ is the SFE of the solid, $\sigma_l$ is the SFE of the liquid and $\sigma_{sl}$ is the SFE of the solid–liquid interface [25].

### 2.5. Electrochemical measurements

Cyclic potentiodynamic polarization tests were performed in PBS (pH = 7.2) at 37 °C ± 1 °C in accordance with ASTM F 2129-08 [24] employing a GAMRY® potentiostat (G-750). A typical three electrode cell consisting of working electrode, reference electrode (saturated calomel electrode, SCE) and carbon as a counter electrode was employed. All tests were conducted at a scan rate of 1.0 mV/s utilizing an exposed working electrode area of 1.0 $cm^2$. The electrolyte was purged with high purity nitrogen for 30 min prior to immersion of the working electrode, as well as continuously during the corrosion test [26].

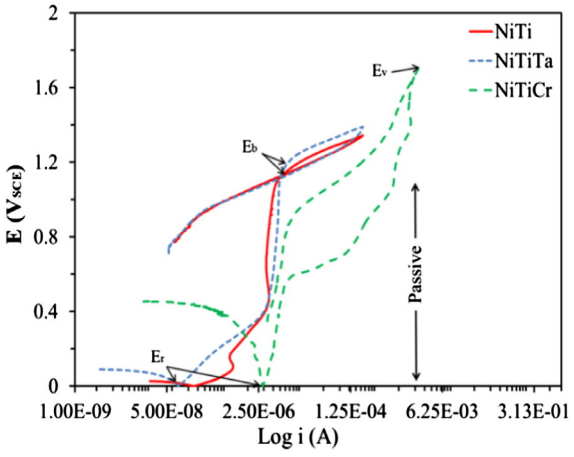


**Fig. 3.** Cyclic potentiodynamic polarization curves for magnetoelectropolished alloys in PBS at 37 °C.

**Table 5**
Average corrosion parameters for alloys tested in PBS at 37 °C as per ASTM: F 2129-08 and ICP-MS analysis.

| Alloy | $E_b$ (V) | $E_r$ (V) | $E_p$ (V) | $E_v$ (V) | $E_b - E_r$ (V) | Ni (ppb) | Ta, Cr (ppb) |
|---|---|---|---|---|---|---|---|
| NiTi | 1.13 | −0.44 | 1.04 | NA | 1.57 | ND | NA |
| NiTi10Ta | 1.15 | −0.38 | 1.14 | NA | 1.53 | ND | ND |
| NiTi10Cr | NA | −0.28 | NA | 1.77 | NA | ND | 1492 |

### 2.6. Nanomechanical evaluation

The bulk hardness and Young's modulus of elasticity were determined using a MTS Nanoindenter XP with a diamond Berkovich indenter. At least 10 indentations spaced 100 μm apart were used to indent the specimens and the modulus and hardness were estimated by adopting the Oliver–Pharr approach [27]. The stiffness was evaluated from the unloading curve by taking the derivative with respect to the displacement, i.e. dP/dh at the point of unloading. The contact area was approximated by a fitting polynomial for a Berkovich tip, the radius of which was calibrated using a tungsten specimen [25]. The area function was calculated for the maximum depth penetrated into the specimen.

### 2.7. Biocompatibility

Two approaches were adopted to assess the biocompatibility of the Nitinol alloys: a) Cytotoxicity of dissolved ions leached from the alloys during corrosion on endothelial cells (cell viability); and b) Cell growth on Nitinol alloys. The alloys were assessed using human pulmonary artery endothelial cells (HPAEC, Fischer Scientific, catalog# PH30205AK) that were maintained in accordance with the instructions provided by the commercial source (Fisher Scientific, catalog# PH30205AK).

#### 2.7.1. Cytotoxicity assessment

The cells were first cultured in a T-75 cell culture flask using F-12K as the medium. When the cells were confluent, they were trypsinized, centrifuged and re-suspended in culture media for cell counting and cell seeding on the binary and ternary MEP treated Nitinol samples. Sulforhodamine B colorimetric assay (SRB, Sigma Aldrich, catalog# TOX6) was used for visualization and cell density measurement. SRB assay provided a method to assess the toxicity of dissolved ions leaching from the Nitinol alloys (into PBS after corrosion tests) on HPAEC cells, hereinafter referred to as corrosion extracts.

Once the cells in the flasks reached 90% confluency, they were trypsinzed and centrifuged. The supernatant was removed and the cell pellet was dissolved in media. Cells were counted using a hemocytometer cell counting device. Additionally, media was further added to achieve a cell concentration of $10^5$ cell/ml. 200 μl of cell solution (approximately 20,000 cells/well) was placed in three 96 well plates.

Endothelial cells in the wells were exposed to three different concentrations of corrosion extracts (10%, 50% and 100%) over periods of 2, 4 and 7 days. The media exposed to cells was prepared by dissolving 10% Fetal Bovine Serum (FBS, ES Cell Qualified, ATCC, catalog# SCRR-30-2020) and 1% Penstrep (Penicillin-Streptomycin Solution, ATCC, catalog#30-2300) into the corrosion extracts. The well plates were then placed in a humidified environment in an incubator at 37 °C under 5% $CO_2$. The viability of the HPAEC was assessed from the absorbance measured after 2, 4 and 7 days.

#### 2.7.2. Cell growth

In order to assess the endothelial cell growth on Nitinol, samples of dimensions ~0.15 in. were placed into each well of a 24-well plate and seeded with $50 \times 10^3$ cells per well. The well plates were then placed in a humidified environment in an incubator at 37 °C under 5% $CO_2$ for 72 h. Later, cell culture media was removed and the samples were gently washed with Dulbecco's phosphate buffered saline (DPBS). 2 ml of Hoechst dye (5 μM) and Mitotracker Red dye (100nM) was added into the wells. The Hoechst dye was used to highlight the nuclei of the cells, while the Mitotracker Red dye was used to highlight the mitochondria of the cells. The plates were again incubated for 20 min, after which the samples were washed three times with DPBS and visualized under an Olympus X fluorescent microscope.

## 3. Results and discussion

### 3.1. Material characterization

The microstructure and phase composition of the alloys were examined by Scanning Electron Microscope (SEM) equipped with an Energy Dispersive Spectrometer (EDS).

After MEP, NiTi samples exhibited a smooth surface as compared with those of Ni–Ti–Ta and Ni–Ti–Cr as shown in the photomicrographs of Fig. 2. It should be noted that after MEP, the grain boundary regions of Ni–Ti–Cr were depressed but those of Ni–Ti–Ta were elevated as shown in the schematic diagrams of Fig. 1(a) and (b) and their photomicrographs in Fig. 2(a), (b) and (c).

Grains of approximately 40 μm in diameter were exposed after MEP of ternary alloys. Additionally, a unique behavior was observed mainly on the grain boundaries of the ternary alloys. For example, EDS analysis

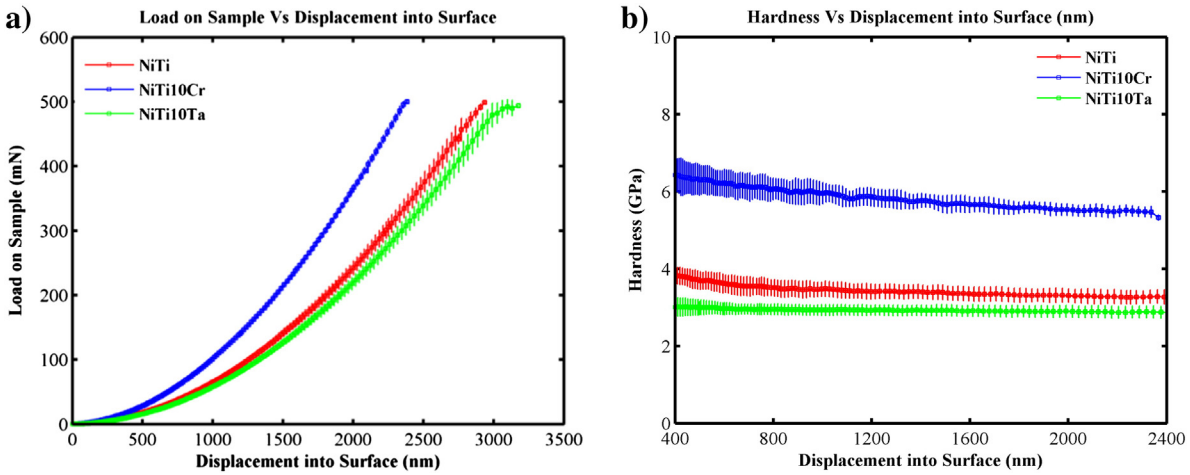


**Fig. 4.** Nanoindentation: (a) Peak load Vs Displacement and (b) Load Vs Hardness curves for Nitinol Alloys.

of Ni–Ti–Ta and Ni–Ti–Cr revealed 66.4 at.% of Ta and 21 at.% of Cr at their grain boundaries respectively. The relatively higher concentration of Ta at the grain boundary was attributed to preferential grain boundary segregation due to its larger atomic radius (~200 pm) relative to that of Cr (~166 pm). Furthermore, during MEP of Nitinol, Ni (ferromagnetic) is preferentially leached from the surface of the alloy as a result of the magnetic field. The presence of dislocations and stress at grain boundaries further exacerbates the leaching of Ni. It should be noted that Ta (paramagnetic) is attracted by the presence of an externally applied magnetic field [28] whereas Cr, though antiferromagnetic at ambient conditions, becomes paramagnetic at 38 °C [28–30]. However, the effect of the magnetic field on Ta and Cr in the ternary alloys was not evaluated in this investigation.

Table 1 shows the nominal and EDS composition of Nitinol alloys, where X represents the ternary elements, tantalum (Ta) and chromium (Cr).

The surface chemistry and depth profile of the Nitinol alloys were examined using XPS. As shown in Table 2, the addition of alloying elements to Nitinol reduced the oxide thickness from 18.2 nm to about 10.4–11.0 nm. The diffusion of elemental nickel from the subsurface layers through the porous $TiO_2$ layer has been reported [31,32]. However, nickel oxide which is less mobile in the $TiO_2$ lattice than metallic nickel, played a significant role in reducing the amount of Ni leached during the corrosion tests. It should be noted that it is not only the amount of nickel present at the surface that governs platelet activation but also its oxidative state [33]. Additionally, the textured surfaces with pore-like features (~50 nm in diameter) observed in Fig. 2 could be favorable for cellular growth. For example, filopodia of endothelial cells can grow into these micro-pores and promote adherence and cell spreading. Tissue integration is facilitated by adhesion and spreading of cells on the surface of implants. Furthermore, micro-pores can act as reservoirs to supply or store nutrients, which are essential for cellular activity [34].

### 3.2. Wettability

The surface properties of a material may depend on the type of surface treatment, which can produce different surface textures, surface chemistries, surface energies and wettabilities, which in turn influence a material's biocompatibility. In order to assess the wettability and surface free energy (SFE) of Nitinol alloys, the contact angle of liquids of different tensions was determined on the surface of the materials. It has been reported that Nitinol's wettability and surface energy significantly influence its biological response [31,35]. Tables 3 and 4 summarize the results of contact angle and surface free energy.

The contact angle of Nitinol alloys changed from hydrophilic (~83.8°) to hydrophobic behavior (~94.7–105.9°) after alloying. The MEP surfaces were more hydrophobic (exhibited a higher contact angle) than the untreated NiTi, as discussed in a previous publication [22].

The thrombogenicity of a material's surface increases with increasing surface energy [35]. Thus, it would appear that NiTi10Cr would be more prone to thrombosis as compared to NiTi10Ta. Furthermore, fibronectin, a key protein involved in cell adhesion is irreversibly adsorbed on hydrophobic surfaces [36]. This implies that ternary Nitinol alloys could better enhance endothelialization than the binary Nitinol which is more hydrophilic.

The importance of polarity on biocompatibility has been investigated by Michiardi et al. where it was deduced that protein and albumin adsorption on Nitinol alloys were directly proportional to the polarity and surface energy and inversely proportional to the concentration of Ni in the bulk alloy [37]. Additionally, Ponsonnet et al. reported that lower SFE corresponds to higher cell growth [36]. The polar (p), dispersion (d) and hydrogen bonding (h) components of surface free energy of Nitinol alloys measured by contact angle meter are presented in Table 4 where it can be seen that each parameter decreased with the addition of alloying element. Furthermore, fractional polarity (FP) was calculated, where fractional polarity = polar / (polar + dispersion). It was previously reported that when a FP is less than 0.3 good cellular adhesion was achieved [15,36]. In this study, the FP ranged between 0.1 and 0.2, which implies that Nitinol is very biocompatible.

**Table 6**
Modulus and hardness calculated from Nanoindentation.

| | NiTi | | NiTi10Cr | | NiTi10Ta | |
|---|---|---|---|---|---|---|
| | E (GPa) | H (GPa) | E (GPa) | H (GPa) | E (GPa) | H (GPa) |
| Mean | 79.4 | 3.6 | 96.7 | 6.3 | 78.9 | 3 |
| Std. dev. | 1.4 | 0.2 | 1.4 | 0.2 | 4.9 | 0.2 |
| % COV | 1.7 | 5.6 | 1.4 | 2.8 | 6.3 | 7.8 |

### 3.3. Cyclic potentiodynamic polarization

Cyclic potentiodynamic polarization curves for Nitinol alloys are depicted in Fig. 3. Two distinct features were observed; a positive and a negative hysteresis. The reverse scan at the vertex potential for NiTi and NiTiTa alloys proceeds initially towards a high current density region with a clockwise loop, whereas in the case of NiTiCr alloys, the reverse scan loops in an anti-clockwise direction (negative hysteresis), i.e., initially the curve proceeds towards a low current density. The corrosion parameters such as breakdown potential ($E_b$), protection potential ($E_p$), vertex potential ($E_v$), rest potential ($E_r$) and the differences between the breakdown and rest potentials ($E_b - E_r$) obtained during cyclic potentiodynamic polarization test are shown in Table 5.

It should be noted that a large hysteresis loop area is associated with a greater disruption of the passive film and lower restoration in surface passivity, which is indicative of a greater risk of localized corrosion. For alloys that exhibit a negative hysteresis (NiTiCr), the corrosion resistance may be evaluated by the vertex potential $E_v$ and is considered more resistant to pitting corrosion [38].

The concentration of dissolved ions in PBS after corrosion was determined by ICP-MS analysis. Little or no metal ion leaching (Ni, Ti and Ta) was detected in the corrosion extract which was attributed to the effect of surface passivation as a result of MEP. These passivating films serve as a protective barrier against metal ion leaching. However, a relatively high concentration of chromium leached from the NiTiCr alloy. This was attributed to surface enrichment of the highly passivating element chromium.

### 3.4. Nanoindentation measurements

Fig. 4(a) shows the plot of Load Vs Displacement at 500 mN and 200 mN peak loads on Nitinol samples. Each sample was indented at

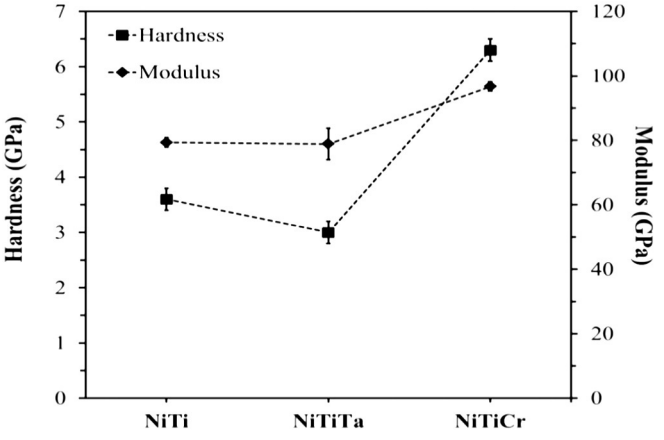


**Fig. 5.** Nanoindentation: hardness and modulus values plotted with respect to composition.

20 locations using different peak loads. Fig. 3(b) shows the modulus and hardness that were calculated using the Oliver–Pharr approach (depths above 1000 nm and peak loads above 25 mN). The modulus of binary Nitinol alloy increased from 79.4 GPa to 96.1 GPa with the addition of Cr, as did the hardness (3.6–6.3 GPa) (see Table 6 and Fig. 5). The addition of Ta decreased the hardness of binary Nitinol whereas the addition of Cr increased its hardness. It has been reported that MEP Nitinol possessed a $TiO_2$ layer that was 10–25 nm thick [22]. Since the oxide layer is relatively thin and the penetration depths (~2400 nm) are of greater magnitude, the parameters evaluated are representative of the bulk.

### 3.5. Biocompatibility studies

The basic mechanisms underlying the interaction between a metal and tissue/blood are still not completely understood and biocompatibility and the hemocompatibility of metallic stents still remain an issue. When a blood vessel is damaged during angioplasty, protein clotting factors and platelets help to repair the damaged site and restore the initial conditions. Fibrinogen adheres onto the damaged vessel where fibrin clots are produced in an effort to reduce blood flow. This cascade of reactions results in the formation of strands of protein called fibrin, which cross-link to form a robust plug, or clot, with platelets and red blood cells trapped within. This process is referred to as thrombosis [39].

The cytotoxicity of dissolved metal ions on endothelial cells was assessed by conducting SRB assays using electrolyte collected after corrosion. All SRB assay results were normalized with respect to fresh media. The SRB assay results revealed that Ni ions exhibited greater toxicity than Cr and Ta ions on endothelial cells. Low cell viability (low SRB values) was observed with NiTi alloys (~0.742) after 1 day of immersion under static immersion. However, higher cell viability was observed with NiTi (~0.933) after 42 days of immersion under static conditions. This was expected due to the low concentration of metal ions released after 42 days of immersion. The average values of 3 SRB assays and the standard deviation error bars are shown in Fig. 6.

The growth of endothelial cells on the surface of Nitinol alloys was assessed using the ISO 10993 protocol for biological evaluation of medical devices. Fig. 7 displays the endothelial cell growth on NiTi, NiTi10Ta and NiTi10Cr where the nuclei (blue) and mitochondria (pink) were monitored.

Good endothelial cell growth was observed on all three surfaces. A confluent monolayer of well-defined cells exhibiting cell-to-cell contact was indicative of a non-cytotoxic response. It was also observed that the diameters of the cell nuclei were greater on Nitinol as compared with those on the ternary Nitinol alloys. As shown in Fig. 8, there was no significant difference in cell growth on each alloy when compared to its untreated counterparts. Each surface displayed excellent endothelial cell growth.

## 4. Conclusions

Enhancing the biocompatibility of a medical device implies a seamless integration into the body with increased health and longevity of the patient. MEP reduced the surface asperities on Nitinol alloys and provided stable oxides on the surface, which significantly improved the corrosion resistance and biocompatibility of the alloys. Ni–Ti–Cr

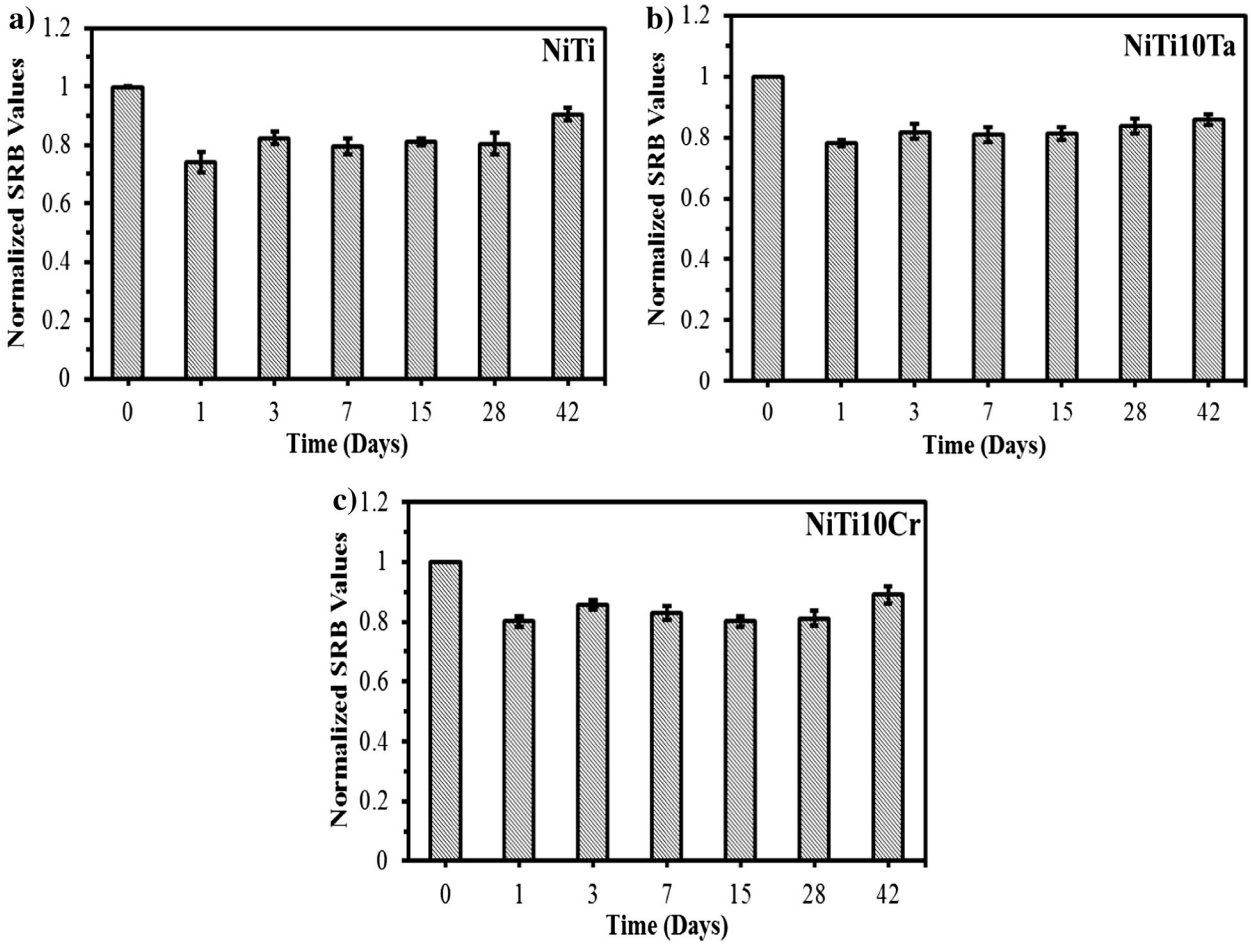


**Fig. 6.** Net growth rate of endothelial cells exposed to dissolved metal ions (static immersion) at 37 °C.

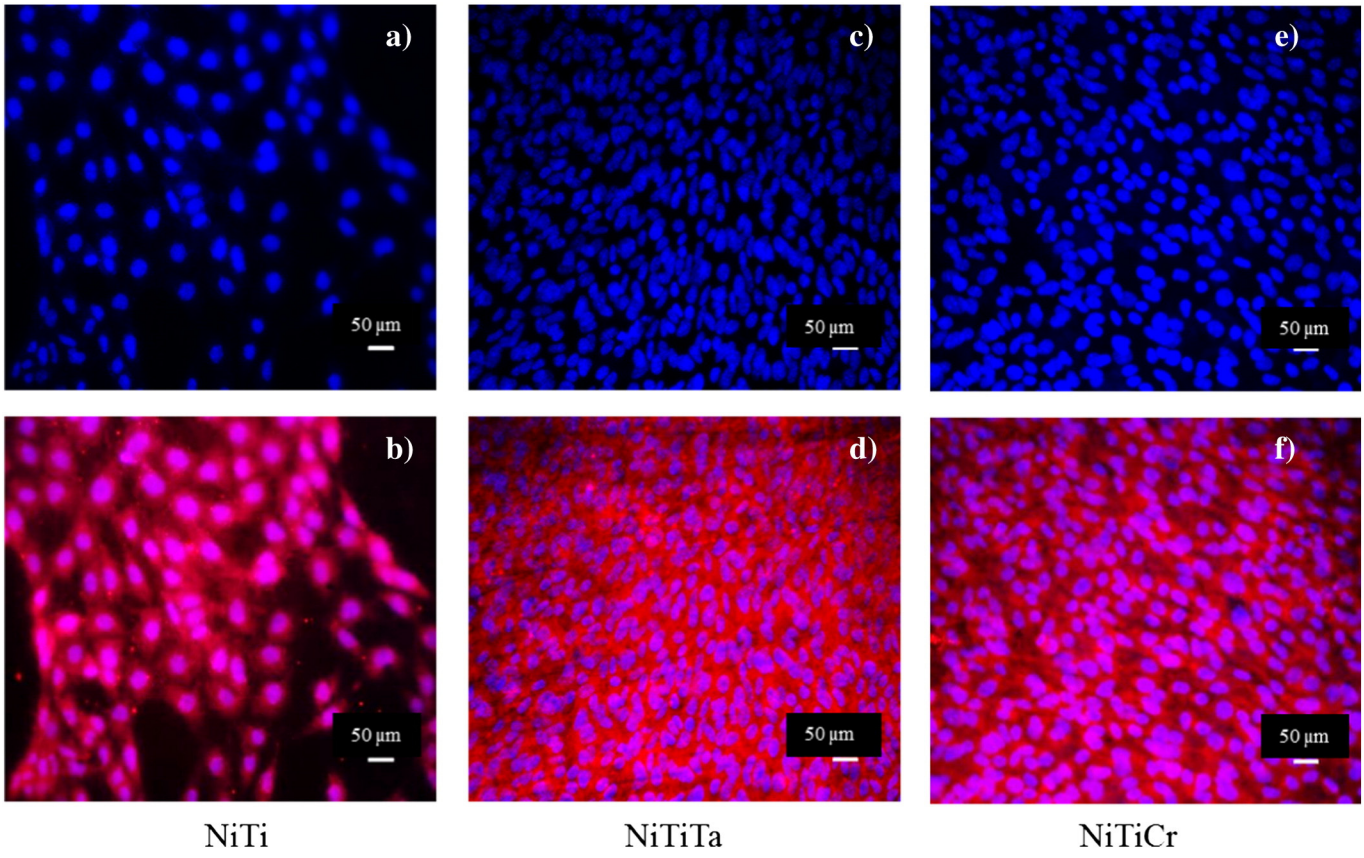


**Fig. 7.** Endothelial cell growth on untreated NiTi (a,b), NiTiTa (c,d) and NiTiCr (e,f). Scale bar — 50 μm.

was more resistant to corrosion and displayed a negative hysteresis, whereas, that of Ni–Ti and Ni–Ti–Ta displayed a positive hysteresis, with the latter being more prone to pitting. High corrosion resistance is one of the main prerequisites for enhanced biocompatibility because it minimizes Ni ion release. The MEP treated alloys formed nickel oxide on their surfaces with no elemental Ni indicating the non-toxic behavior after surface treatment, thereby improving biocompatibility. MEP appears to be a promising technique for improving corrosion resistance as it reduces nickel release and provides a low surface free energy layer that is appropriate for endothelial cell growth. As a consequence, MEP reduces the risk of Ni sensitivity and enhances the biocompatibility of Nitinol alloys.

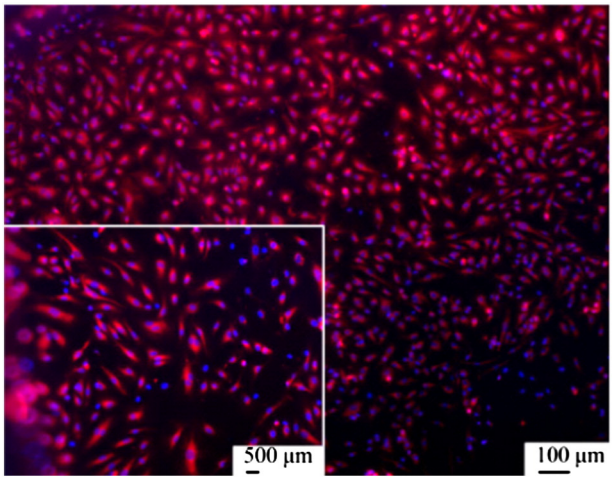


**Fig. 8.** Highlighted nuclei and mitochondria of endothelial cells on magnetoelectropolished NiTi samples.

## Acknowledgments

Puneet Gill acknowledges the Doctoral Evidence Acquisition and Dissertation Year Fellowship awards from the University Graduate School of Florida International University. The authors further acknowledge the facility at Oak Ridge National Laboratory, Tennessee and Advanced Materials Engineering and Research Institute (AMERI) at Florida International University. Norman Munroe would like to acknowledge the financial support from National Institute of General Medical Sciences Award Number SC3GM084816.

## References

[1] T. Bodenheimer, H.H. Pham, Primary care: current problems and proposed solutions, Health Aff. 29 (May 2010) 799.
[2] A.D. Michaels, K. Chatterjee, Angioplasty versus bypass surgery for coronary artery disease, Circulation 106 (December 3, 2002) e187–e190.
[3] P.W. Serruys, H.E. Luijten, K.J. Beatt, R. Geuskens, P.J. Defeyter, M. Vandenbrand, J.H.C. Reiber, H.J. Tenkaten, G.A. Vanes, P.G. Hugenholtz, Incidence of restenosis after successful coronary angioplasty — a time-related phenomenon — a quantitative angiographic study in 342 consecutive patients at 1, 2, 3, and 4 months, Circulation 77 (Feb 1988) 361–371.
[4] G. Dangas, F. Kuepper, Restenosis: repeat narrowing of a coronary artery — prevention and treatment, Circulation 105 (Jun 2002) 2586–2587.
[5] B. Thierry, Y. Merhi, C. Trepanier, L. Bilodcau, L.H. Yahia, M. Tabrizian, Blood compatibility of nitinol compared to stainless steel, In: Proceedings of the Int"l Conference on Shape Memory and Superelastic Technologies NDC Publishers, Pacific Grove, California, 2000, pp. 285–290.
[6] S. Sheth, F. Litvack, V. Dev, M.C. Fishbein, J.S. Forrester, N. Eigler, Subacute thrombosis and vascular injury resulting from slotted-tube nitinol and stainless steel stents in a rabbit carotid artery model, Circulation 94 (October 1, 1996) 1733–1740.
[7] B. Thierry, Y. Merhi, L. Bilodeau, C. Trépanier, M. Tabrizian, Nitinol versus stainless steel stents: acute thrombogenicity study in an ex vivo porcine model, Biomaterials 23 (July 2002) 2997–3005.

[8] J.W. van Werkum, A.A. Heestermans, A.C. Zomer, J.C. Kelder, M.-J. Suttorp, B.J. Rensing, J.J. Koolen, B.R.G. Brueren, J.-H.E. Dambrink, R.W. Hautvast, F.W. Verheugt, J.M. ten Berg, Predictors of coronary stent thrombosis: the Dutch stent thrombosis registry, J. Am. Coll. Cardiol. 53 (2009) 1399–1409.
[9] Donald Cutlip, J. Dawn Abbott, Coronary Artery Stent Thrombosis: Incidence and Risk Factors (UpToDate Ed.), 13 May 2013.
[10] G.L. Buchanan, S. Basavarajaiah, A. Chieffo, Stent thrombosis: incidence, predictors and new technologies, Thrombosis 2012 (2012).
[11] S. Virtanen, I. Milosev, E. Gomez-Barrena, R. Trebse, J. Salo, Y.T. Konttinen, Special modes of corrosion under physiological and simulated physiological conditions, Acta Biomater. 4 (May 2008) 468–476.
[12] R. Rokicki, T. Hryniewicz, K. Rokosz, Modifying metallic implants with magnetoelectropolishing, Medical Device and Diagnostic Industry, 2008. (Available: http://www.mddionline.com/article/modifying-metallic-implants-magnetoelectropolishing).
[13] Y. Shen, G.X. Wang, L. Chen, H. Li, P. Yu, M.J. Bai, Q. Zhang, J. Lee, Q.S. Yu, Investigation of surface endothelialization on biomedical nitinol (NiTi) alloy: effects of surface micropatterning combined with plasma nanocoatings, Acta Biomater. 5 (Nov 2009) 3593–3604.
[14] W. Haider, N. Munroe, V. Tek, C. Pulletikurthi, P.K.S. Gill, S. Pandya, Surface modifications of nitinol, J. Long Term Eff. Med. Implants 19 (07-01-2009) 113–122.
[15] K. Zhang, T. Liu, J.-a. Li, J.-y. Chen, J. Wang, N. Huang, Surface modification of implanted cardiovascular metal stents: from anti-thrombosis and anti-restenosis to endothelialization, J. Biomed. Mater. Res. A 102 (2) (2013) 588–609.
[16] C.L. Chu, C. Guo, X.B. Sheng, Y.S. Dong, P.H. Lin, K.W.K. Yeung, P.K. Chu, Microstructure, nickel suppression and mechanical characteristics of electropolished and photoelectrocatalytically oxidized biomedical nickel titanium shape memory alloy, Acta Biomater. 5 (Jul 2009) 2238–2245.
[17] D. Starosvetsky, I. Gotman, TiN coating improves the corrosion behavior of superelastic NiTi surgical alloy, Surf. Coat. Technol. 148 (2001) 268–276.
[18] D. Zhang, W. Zeng, Z. Zi, P.K. Chu, Corrosion resistance of TiN coated biomedical nitinol under deformation, Mater. Sci. Eng. C 29 (2009) 1599–1603.
[19] S. Shabalovskaya, G. Rondelli, J. Anderegg, J.P. Xiong, M. Wu, Comparative corrosion performance of black oxide, sandblasted, and fine-drawn nitinol wires in potentiodynamic and potentiostatic tests: effects of chemical etching and electropolishing, J. Biomed. Mater. Res. B Appl. Biomater. 69B (2004) 223–231.
[20] D. Persaud-Sharma, N. Munroe, A. McGoron, Electro and magneto-electropolished surface micro-patterning on binary and ternary nitinol, Trends Biomater. Artif. Organs 26 (2012) 74–85.
[21] W. Haider, N. Munroe, Assessment of corrosion resistance and metal ion leaching of nitinol alloys, J. Mater. Eng. Perform. 20 (Jul 2011) 812–815.
[22] W. Haider, Enhanced biocompatibility of NiTi (NITINOL) via surface treatment and alloying(Doctor of Philosophy Dissertation) Mechanical & Materials Engineering, Florida International University, Miami, 2010.
[23] R. Rokicki, W. Haider, T. Hryniewicz, Influence of sodium hypochlorite treatment of electropolished and magnetoelectropolished nitinol surfaces on adhesion and proliferation of MC3T3 pre-osteoblast cells, J. Mater. Sci. Mater. Med. 23 (2012) 2127–2139.
[24] A. International, F2129-08 Standard Test Method for Conducting Cyclic Potentiodynamic Polarization Measurements to Determine the Corrosion Susceptibility of Small Implant Devices, 2008.
[25] D.E. Packham, Work of adhesion: contact angles and contact mechanics, Int. J. Adhes. Adhes. 16 (1996) 121–128.
[26] W. Haider, N. Munroe, C. Pulletikurthi, P.S. Gill, S. Amruthaluri, A comparative biocompatibility analysis of ternary nitinol alloys, J. Mater. Eng. Perform. 18 (08/01/2009) 760–764.
[27] W.C. Oliver, G.M. Pharr, An improved technique for determining hardness and elastic modulus using load and displacement sensing indentation experiments, J. Mater. Res. 7 (1992) 1564–1583.
[28] Tadeusz Hryniewicz, Krzysztof Rokosz, Ryszard Rokicki, Magnetic fields for electropolishing improvement: materials and systems, Int. Lett. Chem. Phys. Astron. 4 (2014) 98–108.
[29] H. Fritzsche, S. Bonn, J. Hauschild, J. Klenke, K. Prokes, G.J. McIntyre, Antiferromagnetic order of thin epitaxial Cr layers in an Fe/Cr(110) multilayer, Phys. Rev. B 65 (2002) 144408.
[30] L.E.T. Feliciano, A.J.A. de Oliveira, W.H. Schreiner, E.C. Pereira, Anomalous magnetic behavior of electrodeposited chromium thin films, J. Electroanal. Chem. 574 (2005) 333–338.
[31] S. Shabalovskaya, J. Anderegg, J. Van Humbeeck, Critical overview of nitinol surfaces and their modifications for medical applications, Acta Biomater. 4 (May 2008) 447–467.
[32] C. Trepanier, M. Tabrizian, L. Yahia, L. Bilodeau, D.L. Piron, Effect of modification of oxide layer on NiTi stent corrosion resistance (vol 43, pg 433, 1998), J. Biomed. Mater. Res. 48 (Spr 1999) 96–98.
[33] D.A. Armitage, D.M. Grant, Characterisation of surface-modified nickel titanium alloys, Mater. Sci. Eng. A Struct. Mater. Prop. Microstruct. Process. 349 (May 2003) 89–97.
[34] S. Oh, C. Daraio, L.H. Chen, T.R. Pisanic, R.R. Finones, S. Jin, Significantly accelerated osteoblast cell growth on aligned TiO2 nanotubes, J. Biomed. Mater. Res. A 78A (Jul 2006) 97–103.
[35] G. Mani, M.D. Feldman, D. Patel, C.M. Agrawal, Coronary stents: a materials perspective, Biomaterials 28 (Mar 2007) 1689–1710.
[36] L. Ponsonnet, K. Reybier, N. Jaffrezic, V. Comte, C. Lagneau, M. Lissac, C. Martelet, Relationship between surface properties (roughness, wettability) of titanium and titanium alloys and cell behaviour, Mater. Sci. Eng. C Biomim. Supramol. Syst. 23 (Jun 2003) 551–560.
[37] A. Michiardi, C. Aparicio, B.D. Ratner, J.A. Planell, J. Gil, The influence of surface energy on competitive protein adsorption on oxidized NiTi surfaces, Biomaterials 28 (Feb 2007) 586–594.
[38] P. Gill, N. Munroe, C. Pulletikurthi, S. Pandya, W. Haider, Effect of manufacturing process on the biocompatibility and mechanical properties of Ti-30Ta alloy, J. Mater. Eng. Perform. 20 (07/01/2011) 819–823.
[39] D.A. Roberts, The Complete Human Body — The Definitive Visual Guide, DK Publishing, New York, 2010..